Modeling and experimental verification of the thermodynamic properties of hydrogen storage materials

Available online at www.sciencedirect.com

ScienceDirect

journal homepage: www.elsevier.com/locate/he

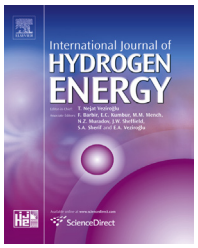

Modeling and experimental verification of the thermodynamic properties of hydrogen storage materials

A.V. Ledovskikh [a], D.L. Danilov [a,b], M. Vliex [a], P.H.L. Notten [a,b,*]

[a] Eindhoven University of Technology, PO Box 513, 5600 MB Eindhoven, The Netherlands
[b] Forschungszentrum Jülich, Fundamental Electrochemistry (IEK-9), D-52425 Jülich, Germany

ARTICLE INFO

Article history:
Received 20 September 2015
Received in revised form
5 November 2015
Accepted 6 November 2015
Available online 26 January 2016

Keywords:
Lattice gas model
Gas phase hydrogen storage
Pressure Composition Isotherms
Thermodynamics
Van 't Hoff

ABSTRACT

A new mathematical model has been developed describing the thermodynamics of the hydrogen absorption and desorption process in Metal Hydrides via the gas phase. This model is based on first principles chemical and statistical thermodynamics and takes into account structural changes occurring inside hydrogen storage materials. A general state equation has been derived considering the chemical potentials of reacting species and volume expansion, from which the equilibrium hydrogen pressure dependence on the absorbed hydrogen content can be calculated. The model is able to predict the classical Van 't Hoff equation from first-principle analytical expressions and gives more insight into the various hydrogen storage characteristics. Pressure-Composition Isotherms have been simulated for various hydride-forming materials. Excellent agreement between simulation results and experimental data has been found in all cases.

Introduction

Metal Hydrides (MH) can be successfully employed as efficient and safe storage media of hydrogen gas. In these materials storage takes place under moderate pressure and temperature conditions. In that respect MH have a significant advantage over traditional hydrogen storage systems, which suffer from either extremely high pressures or very low temperatures. Storage in MH is therefore one of the key factors, facilitating *e.g.* hydrogen-driven fuel cells and Nickel-Metal Hydride (NiMH) batteries [1–7]. In order to unravel the complex hydrogen storage process, a more detailed understanding is, however, essential.

MH materials are generally characterized by pressure-composition isotherms [4–8]. A typical isotherm and corresponding phase diagram for conventional MH alloys are schematically shown in curves (a) and (b) of Fig. 1, respectively [6–9]. The isotherms are generally plotted versus the normalized hydrogen content (x). During hydrogen absorption at low concentrations a solid solution is formed, which is generally denoted by the α-phase. In this concentration region the partial hydrogen pressure ($P^{eq}_{H_2}$) is clearly dependent on the amount of stored hydrogen. After the hydrogen concentration reaches a certain critical value (x_α), phase transition is initiated and the α-phase transforms into the β-phase as indicated in Fig. 2a. The pressure dependence in this two-phase coexistence region is characterized by a (sloping) plateau [10,11].

* *Corresponding author*. Eindhoven University of Technology, PO Box 513, 5600 MB Eindhoven, The Netherlands.
E-mail address: P.H.L.Notten@tue.nl (P.H.L. Notten).

http://dx.doi.org/10.1016/j.ijhydene.2015.11.038

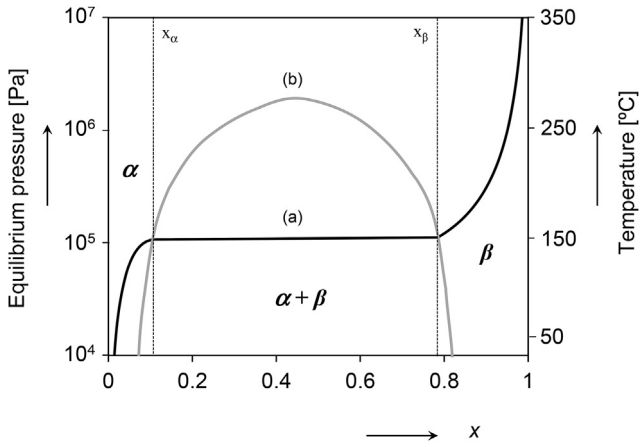

Fig. 1 – Schematic representation of a pressure-composition isotherm (a) and phase-diagram (b) for a typical hydrogen storage material. α and β solid solution regions are indicated together with the temperature-dependent two-phase ($\alpha + \beta$) miscibility gap.

Hydrogen absorption induces significant volumetric expansion of the crystal lattice, especially in two-phase coexistence region, as is schematically represented in Fig. 2b [1–4,12]. After the α-phase has been fully converted into the β-phase at x_β, a clear pressure dependence on x is again found in the solid solution region of the β-phase. The two-phase miscibility gap between x_α and x_β decreases at higher temperatures, to completely disappear at the critical temperature (Fig. 1, curve b). Above the critical temperature there is no two-phase coexistence region [6–9,13,14]. Similarly the critical composition and critical film thickness has been identified at which two-phase coexistence region is absent [12,15].

Several attempts have been made to describe pressure-composition isotherms. Existing mathematical models are often based on statistical thermodynamics, allowing simulating macroscopic characteristics by using microscopic parameters, such as atomic interaction energies, *etc.* One of the first thermodynamic models has been proposed by Lacher [16]. This semi-empirical model successfully described isotherms above the critical temperature but did not give a proper description in the two-phase plateau region. Further improvements of the Lacher-model have been proposed by others [17,18]. These models are, however, based on heuristic assumptions and empirical parameters, and have a high level of mathematical complexity. A different approach has been adopted by Flanagan et al. [3,10,11] who described the thermodynamics of the hydrogen storage system in terms of chemical potential of reactants and reaction products. Similar model with simple atomic interaction energy term has been proposed by McKinnon [19]. Unfortunately these models can only describe isotherms with flat plateau regions, using the so-called Maxwell construction. Attempts to describe sloping plateaus were, however, rather empirical [20].

Recently a Lattice Gas Model (LGM) has been proposed for MH systems [7]. The advantage of this LGM is that phase transitions are included together with (inter-phase)

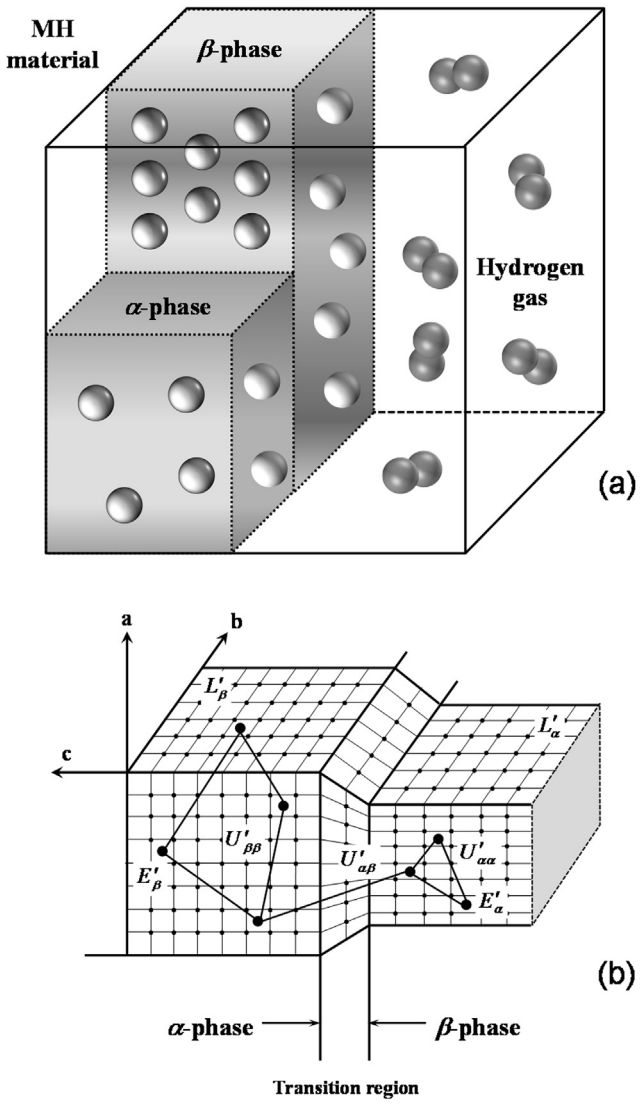

Fig. 2 – (a) Schematic representation of the hydrogen storage process. (b) Schematic representation of the lattice gas model in the two-phase ($\alpha + \beta$) coexistence region for a typical hydrogen storage material. The various host energies (L'_i), hydrogen guest energies (E'_i) and interaction energies (U'_{ij}) between hydrogen stored in the different phases are indicated.

interaction energies of hydrogen inside the host material (see Fig. 2b). The excellent agreement between simulation results and experimental data has been shown for various types of MH materials revealing both flat and sloping plateaus [7,15,21]. The original LGM has, however, been developed with the assumption that the change of the Gibbs free energy during the (de)hydrogenation process depends on the materials solid-state properties only and other contributions were therefore neglected. Consequently, the LGM was not able to describe the characteristics of complete hydrogen storage systems, hence excluding the possibility to simulate, for example, the Van 't Hoff equation [5,22].

In the present paper, a comprehensive model is proposed, describing the thermodynamics of complete MH systems. This model is based on first principles of statistical and classical thermodynamics and is a generalization of the previous LGM, implying that contributions of all species involved in the (de)hydrogenation process are included together with the pressure dependence and materials volume expansion. The simulation results will be compared with experimental results.

Model description

System definition

Gas phase hydrogen storage is a complex multi-stage process, which is schematically represented in Fig. 2 a. Dissociation of hydrogen molecules at the interface of the metal and the gas phase results in atomically adsorbed hydrogen. Subsequently, hydrogen is absorbed in the bulk of the MH where hydrogen atoms occupy interstitial sites of the host material. The overall reaction, taking place during hydrogen absorption/desorption can, in general terms, be given by

$$M + \frac{1}{2}H_2 \leftrightarrow MH, \tag{1}$$

where the unhydrided host material is represented by M. (De) Hydrogenation generally takes place in a closed container with fixed volume.

According to the Lattice Gas approach the bulk of the MH material can be considered as a host-guest system in which hydrogen guest atoms can occupy the host sites [6,7]. It has been argued that each host site can either be occupied by a single hydrogen atom or is empty. Consider the bulk of a hydride-forming material to consist of M unit cells, which are during the hydrogen storage process either in the α- (M_α) or the β-phase (M_β). For many MH compounds the crystallographic structure of both phases are identical and M therefore remains constant during the absorption/desorption process

$$M = M_\alpha + M_\beta. \tag{2}$$

When furthermore is assumed that the numbers of host sites per unit cell (d) in both the α- and β-phase are equal, the total number of host sites in the present hydride-forming system (N) can be represented by

$$N = N_\alpha + N_\beta = d\cdot M_\alpha + d\cdot M_\beta. \tag{3}$$

Denoting the number of hydrogen guest atoms in the α- and β-phases as n_α and n_β, respectively, the total number of occupied sites (n) is then given by $n = n_\alpha + n_\beta$. The normalized number of absorbed hydrogen atoms (x) can be represented by

$$x = \frac{n}{n_{\max}} = \frac{n_\alpha + n_\beta}{n_{\max}}, \tag{4}$$

where n_{max} is the maximal number of occupied host sites. Assuming a linear dependence of the number of unit cells during phase transition (see Ref. [7]), N_α and N_β can be represented as function of the normalized hydrogen content, according to

$$N_\alpha = M_\alpha d = \begin{cases} Md, & x < x_\alpha \\ Md\left(\dfrac{x_\beta - x}{x_\beta - x_\alpha}\right), & x_\alpha \le x \le x_\beta \\ 0, & x > x_\beta \end{cases},$$
$$N_\beta = M_\beta d = \begin{cases} 0, & x < x_\alpha \\ Md\left(\dfrac{x - x_\alpha}{x_\beta - x_\alpha}\right), & x_\alpha \le x \le x_\beta \\ Md, & x > x_\beta \end{cases} \tag{5}$$

where x_α and x_β are the phase transition points (Fig. 1). Similarly, n_α and n_β can be represented as a function of x

$$n_\alpha = \begin{cases} xn_{\max}, & x < x_\alpha \\ x_\alpha n_{\max}\left(\dfrac{x_\beta - x}{x_\beta - x_\alpha}\right), & x_\alpha \le x \le x_\beta \\ 0, & x > x_\beta \end{cases},$$
$$n_\beta = \begin{cases} 0, & x < x_\alpha \\ x_\beta n_{\max}\left(\dfrac{x - x_\alpha}{x_\beta - x_\alpha}\right), & x_\alpha \le x \le x_\beta \\ xn_{\max}, & x > x_\beta \end{cases} \tag{6}$$

The total Gibbs free energy (G_{MH}[J]) of the MH system can be written as [23–25].

$$G_{MH} = G_H + G_{M_\alpha} + G_{M_\beta} + G_{H_2}, \tag{7}$$

where G_H is the Gibbs free energy of hydrogen absorbed in the host material, G_{M_α} and G_{M_β} are the Gibbs free energies of the metal host lattice (M) for the α and β phase, respectively, and G_{H_2} is the Gibbs free energy of hydrogen (H_2) in the gas phase. Each term in Eq. (7) is the product of the chemical potential (μ_i [J mol^{-1}]) and the number of moles (ν_i) involved [25,26], according to

$$G_i = \nu_i \mu_i, \tag{8}$$

where index i indicates the various components of the hydrogen-storage system, *i.e.* $i = H$, M_α, M_β, H_2.

During the (de)hydrogenation process the molar amount of hydrogen changes in each part of the system together with the equilibrium gas-phase hydrogen pressure (P_{H_2} [Pa]) and the temperature (T [K]). The increment of the total Gibbs free energy for the (de)hydrogenation process (Eq. (1)) must therefore be taken into account [23–26], which leads to

$$dG_{MH} = \left(\frac{\partial G_{MH}}{\partial \nu_H}\right)_{T,P_{H_2},\nu_{M_\alpha},\nu_{M_\beta},\nu_{H_2}} d\nu_H + \left(\frac{\partial G_{MH}}{\partial \nu_{M_\alpha}}\right)_{T,P_{H_2},\nu_H,\nu_{M_\beta},\nu_{H_2}} d\nu_{M_\alpha}$$
$$+ \left(\frac{\partial G_{MH}}{\partial \nu_{M_\beta}}\right)_{T,P_{H_2},\nu_H,\nu_{M_\alpha},\nu_{H_2}} d\nu_{M_\beta} + \left(\frac{\partial G_{MH}}{\partial \nu_{H_2}}\right)_{T,P_{H_2},\nu_{MH},\nu_{M_\alpha},\nu_{M_\beta}} d\nu_{H_2}$$
$$+ \left(\frac{\partial G_{MH}}{\partial P_{H_2}}\right)_{T,\nu_H,\nu_{M_\alpha},\nu_{M_\beta},\nu_{H_2}} dP_{H_2} + \left(\frac{\partial G_{MH}}{\partial T}\right)_{P_{H_2},\nu_H,\nu_{M_\alpha},\nu_{M_\beta},\nu_{H_2}} dT. \tag{9}$$

Obviously, under isothermal conditions, the temperature is constant and the last term of Eq. (9) is zero. According to general thermodynamics, the system is in equilibrium when $dG_{MH} = 0$ [25,26]. When furthermore, the definition of the chemical

potential $\mu_i = (\partial G_i/\partial \nu_i)_{T,\,P_{H_2},\nu_j}$ is taken into account, Eqs. (8) and (9) can be rewritten under equilibrium conditions as

$$dG_{MH} = \mu_H d\nu_H + \mu_{M_\alpha} d\nu_{M_\alpha} + \mu_{M_\beta} d\nu_{M_\beta} + \mu_{H_2} d\nu_{H_2} + \left(\frac{\partial G_{MH}}{\partial P_{H_2}}\right)_{T,\nu_H,\nu_{M_\alpha},\nu_{M_\beta},\nu_{H_2}} dP_{H_2} = 0. \tag{10}$$

The equilibrium condition of Eq. (10) can now be connected to the microscopic parameters of the hydrogen storage system. Considering the general expression for the Gibbs free energy, $G = H - TS$, the chemical potentials of each component in the system can be expressed by

$$\mu_i = \left(\frac{\partial G_i}{\partial \nu_i}\right)_{T,P_{H_2},\nu_j} = \left(\frac{\partial H_i}{\partial \nu_i}\right)_{T,P_{H_2}} - T\left(\frac{\partial S_i}{\partial \nu_i}\right)_{T,P_{H_2}}, \tag{11}$$

where H_i [J] is the enthalpy and S_i [J K^{-1}] the entropy. As the enthalpy can be described by $H = U + PV$, Eq. (11) can be expanded to

$$\mu_i = \left(\frac{\partial G_i}{\partial \nu_i}\right)_{T,P_{H_2},\nu_j} = \left(\frac{\partial U_i}{\partial \nu_i}\right)_{T,P_{H_2},\nu_j} - T\left(\frac{\partial S_i}{\partial \nu_i}\right)_{T,P_{H_2}} + P_{H_2}\left(\frac{\partial V_i}{\partial \nu_i}\right)_{T,P_{H_2},\nu_j}, \tag{12}$$

in which U_i [J] is the internal energy and V_i [m^3] is the volume of the component under consideration. Eq. (12) will be derived below for each component in the system.

Hydrogen in the solid ($\mu_H d\nu_H$)

The first term in Eq. (12) requires the total internal energy of hydrogen absorbed in the hydride-forming material (U_H). The so-called Bragg-Williams approximation has been adopted, implying that the absorbed hydrogen atoms are randomly distributed in the host material [27]. E_i [eV] represents the energy of the individual hydrogen atoms absorbed in both the α and β phase as indicated in Fig. 2b. It is assumed that the hydrogen atom absorbed at a particular site can interact with hydrogen atoms at any other sites with a characteristic interaction energy. According to the mean-field approximation the interaction energy between the occupied sites does not depend on their location. $U_{\alpha\alpha}$ and $U_{\beta\beta}$ [eV] correspond to the attraction or repulsion energies of H-atoms in the α- and β-phase, respectively. $U_{\alpha\beta}$ represents that between H-atoms in the different phases (Fig. 2b). Taking the amount of hydrogen in each phase into account, U_H can be described by

$$U_H = e\left\{E_\alpha n_\alpha + E_\beta n_\beta + \frac{U_{\alpha\alpha}}{2n_{max}} n_\alpha^2 + \frac{U_{\beta\beta}}{2n_{max}} n_\beta^2 + \frac{U_{\alpha\beta}}{2n_{max}} n_\alpha n_\beta\right\}, \tag{13}$$

where n_i has been defined by Eq. (6) and e is the elementary charge ($1.6\cdot10^{-19}$ C) [23]. Eq. (12) requires the derivative of U_H with respect to the amount of absorbed hydrogen (ν_H). However n_i are functions of normalized hydrogen concentration. Considering the normalized hydrogen concentration x, ν_H can be represented by

$$\nu_H = \frac{n_{max}}{N_A} x, \tag{14}$$

leading to

$$\left(\frac{\partial U_H}{\partial \nu_H}\right)_{T,P_{H_2}} = \frac{N_A}{n_{max}}\left(\frac{\partial U_H}{\partial x}\right)_{T,P_{H_2}} = F\varepsilon_H, \tag{15}$$

where N_A is Avogadro's number, F ($= eN_A$) the Faraday constant and ε_H [eV] is defined as

$$\varepsilon_H = \begin{cases} E_\alpha + U_{\alpha\alpha}x, & x < x_\alpha \\ \dfrac{E_\beta x_\beta - E_\alpha x_\alpha - U_{\alpha\alpha}x_\alpha^2(N_\alpha/n_{max}) + U_{\beta\beta}x_\beta^2(N_\beta/n_{max}) + U_{\alpha\beta}x_\alpha x_\beta(N_\alpha/n_{max} - N_\beta/n_{max})/2}{x_\beta - x_\alpha}, & x_\alpha \le x \le x_\beta \\ E_\beta + U_{\beta\beta}x, & x > x_\beta \end{cases} \tag{16}$$

in both solid solutions ($x < x_\alpha$ and $x > x_\beta$) and the two-phase coexistence region ($x_\alpha \le x \le x_\beta$).

The second term in Eq. (12) requires the entropy of absorbed hydrogen in the three crystallographic regions, which can be obtained from the Bolzmann equation [7].

$$S_H = -kn_{max}\begin{cases} x\ln x + (1-x)\ln(1-x), & x < x_\alpha \\ S_\alpha^0\left(\dfrac{x_\beta - x}{x_\beta - x_\alpha}\right) + S_\beta^0\left(\dfrac{x - x_\alpha}{x_\beta - x_\alpha}\right), & x_\alpha \le x \le x_\beta, \\ x\ln x + (1-x)\ln(1-x), & x > x_\beta \end{cases} \tag{17}$$

where k is the Boltzmann constant ($1.38\cdot10^{-23}$ J K^{-1}). The partial entropies in the plateau region (S_i^0) can conveniently be expressed as a function of x_α and x_β, according to

$$S_i^0 = x_i \ln x_i + (1 - x_i)\ln(1 - x_i), \tag{18}$$

where i again refers to the individual crystallographic phases. Differentiating S_H in Eq. (17) with respect to the molar amount of absorbed hydrogen and taking Eq. (14) into account yields

$$s_H = \left(\frac{\partial S_H}{\partial \nu_H}\right)_{T,\,P_{H_2}} = \frac{N_A}{n_{max}}\left(\frac{\partial S_H}{\partial x}\right)_{T,\,P_{H_2}} = R\begin{cases} \ln\left(\dfrac{1-x}{x}\right), & x < x_\alpha \\ \dfrac{S_\alpha^0 - S_\beta^0}{x_\beta - x_\alpha}, & x_\alpha \le x \le x_\beta, \\ \ln\left(\dfrac{1-x}{x}\right), & x > x_\beta \end{cases} \tag{19}$$

where $R = kN_A = 8.31$ [J mol^{-1} K^{-1}], is the gas constant [23]. Substituting Eqs. (15) and (19) into Eq. (12) leads to the following expression for the chemical potential of absorbed hydrogen

$$\mu_H = F\varepsilon_H - Ts_H + P_{H_2}\left(\frac{\partial V_H}{\partial \nu_H}\right)_{T,P_{H_2},\nu_{M_\alpha},\nu_{M_\beta}}, \tag{20}$$

which, after multiplication by the increment $d\nu_H$, forms the first term in Eq. 10

$$\mu_H d\nu_H = \left(F\varepsilon_H - Ts_H + P_{H_2}\left(\frac{\partial V_H}{\partial \nu_H}\right)_{T,P_{H_2},\nu_{M_\alpha},\nu_{M_\beta}}\right) d\nu_H. \tag{21}$$

Host lattice contribution ($\mu_{M_\alpha} d\nu_{M_\alpha} + \mu_{M_\beta} d\nu_{M_\beta}$)

Consider the internal energy of the host lattice U_{Mi} [J] of both crystallographic phases. Denoting the energy contribution of each unit cell by L_i [eV] (Fig. 2b), the internal energy of the host material can be represented by

$$U_{M_i} = eL_iM_i, \tag{22}$$

where the number of unit cells (M_i) in each phase satisfies Eq. (5). Obviously, in the solid solution regions of both the α- and β-phase M_i is constant, consequently $(\partial U_{M_i}/\partial \nu_{M_i})_{T,\,P_{H_2}} = 0$. In the two-phase coexistence region the derivative $(\partial U_{M_i}/\partial \nu_{M_i})_{T,\,P_{H_2}}$ can be calculated, taking into account that $\nu_{M_i} = \frac{M_i}{N_A}$, which leads to

$$\left(\frac{\partial U_{M_i}}{\partial \nu_{M_i}}\right)_{T,P_{H_2}} = N_A\left(\frac{\partial U_{M_i}}{\partial M_i}\right)_{T,P_{H_2}} = FL_i. \tag{23}$$

As the host material is assumed to be crystalline, its entropy can be considered constant [25], therefore $(\partial S_{M_i}/\partial \nu_{M_i})_{T,\,P_{H_2}} = 0$. Obviously, the derivative of ν_{M_i} is zero when M_i is not present in the system. The following expressions for the chemical potentials therefore hold in the three crystallographic regions

$$\mu_{M_\alpha} = \begin{cases} P_{H_2}\left(\dfrac{\partial V_{M_\alpha}}{\partial \nu_{M_\alpha}}\right)_{T,\,P_{H_2},M_\beta}, & x \le x_\alpha \\ FL_\alpha + P_{H_2}\left(\dfrac{\partial V_{M_\alpha}}{\partial \nu_{M_\alpha}}\right)_{T,\,P_{H_2},M_\beta}, & x_\alpha < x \le x_\beta \\ 0, & x > x_\beta \end{cases}, \quad \mu_{M_\beta}$$
$$= \begin{cases} 0, & x \le x_\alpha \\ FL_\beta + P_{H_2}\left(\dfrac{\partial V_{M_\beta}}{\partial \nu_{M_\beta}}\right)_{T,\,P_{H_2},M_\alpha}, & x_\alpha < x \le x_\beta \\ P_{H_2}\left(\dfrac{\partial V_{M_\beta}}{\partial \nu_{M_\beta}}\right)_{T,\,P_{H_2},M_\alpha}, & x > x_\beta \end{cases}. \tag{24}$$

According to the definition of Eq. (2) the total number of unit cells in the present MH-system remains constant during the hydride-formation process, implying that

$$\nu_M = \nu_{M_\alpha} + \nu_{M_\beta}, \tag{25}$$

and hence that

$$d\nu_{M_\alpha} = -d\nu_{M_\beta}. \tag{26}$$

In the two-phase coexistence region Eqs. (25) and (26) imply that

$$d\nu_{M_\alpha} = -d\nu_{M_\beta} = -\frac{d\nu_H}{d}, \tag{27}$$

The summation of the second and third term in Eq. (10) can then be written as Eq. (28)

$$\mu_{M_\alpha} d\nu_{M_\alpha} + \mu_{M_\beta} d\nu_{M_\beta} = d\nu_H \begin{cases} 0, & x \le x_\alpha \\ FL + P_{H_2}\left[\dfrac{1}{d}\left(\dfrac{\partial V_{M_\beta}}{\partial \nu_{M_\beta}}\right)_{T,\,P_{H_2},\nu_{M_\beta}} - \dfrac{1}{d}\left(\dfrac{\partial V_{M_\alpha}}{\partial \nu_{M_\alpha}}\right)_{T,\,P_{H_2},\nu_{M_\alpha}}\right], & x_\alpha < x \le x_\beta \\ 0, & x > x_\beta \end{cases}. \tag{28}$$

in which $L = \frac{L_\beta - L_\alpha}{d}$.

Hydrogen in the gas phase ($\mu_{H_2} d\nu_{H_2}$)

Considering hydrogen as a di-atomic ideal gas, the chemical potential μ_{H_2} under isothermal conditions has been derived to be

$$\mu_{H_2} = RT\left(\frac{7}{2} - s_0\right) + RT\ln\frac{P_{H_2}}{P_{ref}}, \tag{29}$$

where P_{ref} is the reference pressure (10^5 [Pa]). Note that Rs_0 defines the molar entropy of hydrogen gas under standard conditions. Eq. (29) represents a generalization of the classic expression for the chemical potential of monoatomic ideal gases given in Ref. [28]. Its derivation can be found in Appendix I for the convenience of reader.

Considering a closed system in which the total amount of atomic hydrogen (ν_{tot} [mol]) in the system is constant, the conservation law requires that

$$\nu_{tot} = \nu_H + 2\nu_{H_2}, \tag{30}$$

where the stoichiometric coefficient 2 converts the amount of molecular hydrogen into atomic hydrogen. In this equilibrium situation any change in the amount of hydrogen in the solid can only be achieved at the expense of the gas phase hydrogen, *i.e.*

$$d\nu_{H_2} = -\frac{1}{2}d\nu_H. \tag{31}$$

Therefore the fourth term in Eq. (10) can be represented by

$$\mu_{H_2} d\nu_{H_2} = -\frac{1}{2}\left(RT\left(\frac{7}{2} - s_0\right) + RT\ln\frac{P_{H_2}}{P_{ref}}\right)d\nu_H. \tag{32}$$

Pressure-related term ($(\partial G/\partial P_{H_2})_{T,\nu_{H_2},\nu_H,\nu_M} dP_{H_2}$)

Consider the pressure-related term in Eq. (10), which includes the partial derivative of the Gibbs free energy with respect to the gas-phase hydrogen pressure $(\partial G/\partial P_{H_2})_{T,\nu_{H_2},\nu_H,\nu_M} dP_{H_2}$. According to the ideal gas law [23–25] the hydrogen pressure can be expressed in terms of the amount of hydrogen in the gas phase, according to

$$V_g P_{H_2} = \nu_{H_2} RT, \tag{33}$$

where V_g is the volume of the gas phase. Due to the volume expansion of the hydride-forming material, which sometimes can be quite significant [4,12], V_g may change during the (de) hydrogenation process in a fixed container. Using Eq. (31), Eq. (33) can be rewritten as

$$V_g \cdot dP_{H_2} + P_{H_2} \cdot dV_g = -\frac{1}{2} RT \cdot d\nu_H, \tag{34}$$

from which the total pressure increment can be obtained

$$dP_{H_2} = -\frac{1}{V_g}\left[\frac{1}{2}RT + P_{H_2}\frac{dV_g}{d\nu_H}\right] d\nu_H. \tag{35}$$

The partial derivative of the Gibbs free energy with respect to hydrogen pressure can be found, using the definition of Eq. (29) and that of the ideal gas (Eq. (33)) [25], according to

$$\left(\frac{\partial G}{\partial P_{H_2}}\right)_{T,\nu_H,\nu_{M_\alpha},\nu_{M_\beta},\nu_{H_2}} = \left(\frac{\partial\left(\nu_{H_2}\mu_{H_2}\right)}{\partial P_{H_2}}\right)_{T,\nu_H,\nu_{M_\alpha},\nu_{M_\beta},\nu_{H_2}} = \nu_{H_2}\left(\frac{\partial \mu_{H_2}}{\partial P_{H_2}}\right)_{T,\nu_H,\nu_{M_\alpha},\nu_{M_\beta},\nu_{H_2}} = \nu_{H_2}\frac{RT}{P_{H_2}} = V_g. \tag{36}$$

Combining Eqs. (35) and (36), the following expression is obtained

$$\left(\frac{\partial G}{\partial P_{H_2}}\right)_{T,\nu_H,\nu_{M_\alpha},\nu_{M_\beta},\nu_{H_2}} dP_{H_2} = -\left[\frac{1}{2}RT + P_{H_2}\frac{dV_g}{d\nu_H}\right] d\nu_H. \tag{37}$$

Obviously for isothermal measurements, for example by making use of Sievert-type equipment, the total volume of the entire hydrogen storage system is considered constant. The change in the free gas volume can therefore be expressed in terms of the volume change of the solid which, in turn, depends on the stored hydrogen content inside the solid. This is dependent on the materials volume expansion.

Equilibrium condition (dG = 0)

According to the general condition of equilibrium (Eq. (10)) the Gibbs free energy is minimum when $dG = 0$. Introducing Eqs. ((21), (28), (32) and (37)) into Eq. (10) the following Eq. (38) is obtained.

Obviously, Eq. (38) requires the bracketed terms to be zero, which yields after rearrangements Eq. (39).

Eq. (39) represents the general state equation for hydrogen storage systems and includes the gas phase, the host material and hydrogen absorbed inside the various crystallographic phases of the host material. It describes hydrogen absorption/desorption isotherms in its most general form, taking into account hydrogen pressure changes and materials volume expansion, and connects microscopic materials properties with macroscopic characteristics, such as pressure and volume, which can be measured experimentally. Eq. (39) can be solved analytically with respect to P_{H_2} using the so-called Lambert W-function [29]. Denote

$$dG_{H_2} = 0 = \begin{cases} \left\{-\frac{1}{2}RT - P_{H_2}\left[\frac{dV_g}{d\nu_H} - \left(\frac{\partial V_H}{\partial \nu_H}\right)_{T,P_{H_2},\nu_{M_\alpha},\nu_{M_\beta}}\right] - \frac{1}{2}\left(RT\left(\frac{7}{2} - s_0\right) + RT\ln\frac{P_{H_2}}{P_{ref}}\right) + F\varepsilon_H - Ts_H\right\} d\nu_H, & x \le x_\alpha \\ \left\{-\frac{RT}{2} - P_{H_2}\left[\frac{dV_g}{d\nu_H} - \frac{1}{d}\left(\frac{\partial V_{M_\beta}}{\partial \nu_{M_\beta}}\right)_{T,P_{H_2},\nu_{M_\alpha}} + \frac{1}{d}\left(\frac{\partial V_{M_\alpha}}{\partial \nu_{M_\alpha}}\right)_{T,P_{H_2},\nu_{M_\beta}} - \left(\frac{\partial V_H}{\partial \nu_H}\right)_{T,P_{H_2},\nu_{M_\alpha},\nu_{M_\beta}}\right] + FL - \frac{1}{2}\left(RT\left(\frac{7}{2} - s_0\right) + RT\ln\frac{P_{H_2}}{P_{ref}}\right) + F\varepsilon_H - Ts_H\right\} d\nu_H, & x_\alpha < x \le x_\beta \\ \left\{-\frac{1}{2}RT - P_{H_2}\left[\frac{dV_g}{d\nu_H} - \left(\frac{\partial V_H}{\partial \nu_H}\right)_{T,P_{H_2},\nu_{M_\alpha},\nu_{M_\beta}}\right] - \frac{1}{2}\left(RT\left(\frac{7}{2} - s_0\right) + RT\ln\frac{P_{H_2}}{P_{ref}}\right) + F\varepsilon_H - Ts_H\right\} d\nu_H, & x > x_\beta \end{cases} \tag{38}$$

$$0 = \begin{cases} \left\{-\frac{RT}{2} - \frac{1}{2}\left(RT\left(\frac{7}{2} - s_0\right) + RT\ln\frac{P_{H_2}}{P_{ref}}\right) + F\varepsilon_H - Ts_H - P_{H_2}\left[\frac{dV_g}{d\nu_H} - \left(\frac{\partial V_H}{\partial \nu_H}\right)_{T,P_{H_2},\nu_{M_\alpha},\nu_{M_\beta}}\right]\right\}, & x \le x_\alpha \\ \left\{-\frac{RT}{2} - \frac{1}{2}\left(RT\left(\frac{7}{2} - s_0\right) + RT\ln\frac{P_{H_2}}{P_{ref}}\right) + F\varepsilon_H - Ts_H + FL - P_{H_2}\left[\frac{dV_g}{d\nu_H} - \frac{1}{d}\left(\frac{\partial V_{M_\beta}}{\partial \nu_{M_\beta}}\right)_{T,P_{H_2},\nu_{M_\alpha}} + \frac{1}{d}\left(\frac{\partial V_{M_\alpha}}{\partial \nu_{M_\alpha}}\right)_{T,P_{H_2},\nu_{M_\beta}} - \left(\frac{\partial V_H}{\partial \nu_H}\right)_{T,P_{H_2},\nu_{M_\alpha},\nu_{M_\beta}}\right]\right\}, & x_\alpha < x \le x_\beta \\ \left\{-\frac{RT}{2} - \frac{1}{2}\left(RT\left(\frac{7}{2} - s_0\right) + RT\ln\frac{P_{H_2}}{P_{ref}}\right) + F\varepsilon_H - Ts_H - P_{H_2}\left[\frac{dV_g}{d\nu_H} - \left(\frac{\partial V_H}{\partial \nu_H}\right)_{T,P_{H_2},\nu_{M_\alpha},\nu_{M_\beta}}\right]\right\}, & x > x_\beta \end{cases} \tag{39}$$

$$\lambda = \begin{cases} \dfrac{dV_g}{d\nu_H} - \left(\dfrac{\partial V_H}{\partial \nu_H}\right)_{T,P_{H_2},\nu_{M_\alpha},\nu_{M_\beta}}, & x \le x_\alpha \\ \dfrac{dV_g}{d\nu_H} - \dfrac{1}{d}\left(\dfrac{\partial V_{M_\beta}}{\partial \nu_{M_\beta}}\right)_{T,P_{H_2},\nu_{M_\alpha}} + \dfrac{1}{d}\left(\dfrac{\partial V_{M_\alpha}}{\partial \nu_{M_\alpha}}\right)_{T,P_{H_2},\nu_{M_\beta}} - \left(\dfrac{\partial V_H}{\partial \nu_H}\right)_{T,P_{H_2},\nu_{M_\alpha},\nu_{M_\beta}}, & x_\alpha < x \le x_\beta, \\ \dfrac{dV_g}{d\nu_H} - \left(\dfrac{\partial V_H}{\partial \nu_H}\right)_{T,P_{H_2},\nu_{M_\alpha},\nu_{M_\beta}}, & x > x_\beta \end{cases} \quad (40)$$

then equilibrium hydrogen pressure enters Eq. (39) in the linear ($-P_{H_2}\lambda$) and in the logarithmic terms ($-\frac{1}{2}RT\ln\frac{P_{H_2}}{P_{ref}}$). Introducing new variables Eq. (39) can be written in the following form:

$$-z(x) + aY + b\ln Y = 0, \quad (41)$$

where $Y = \frac{P_{H_2}}{P_{ref}}$; $a = -P_{ref}\lambda$; $b = -\frac{1}{2}RT$ and function $z(x)$ is defined as

$$z(x) = \begin{cases} -\left[F(\varepsilon_H - \varepsilon_M) - T\left(s_H - \frac{1}{2}Rs_0\right) - \frac{9}{4}RT - FL\right], & x_\alpha \le x \le x_\beta \\ -\left[F(\varepsilon_H - \varepsilon_M) - T\left(s_H - \frac{1}{2}Rs_0\right) - \frac{9}{4}RT\right], & otherwise \end{cases} \quad (42)$$

Eq. (41) can be further rearranged with respect to the normalized pressure term Y as

$$cY\cdot\exp(cY) = cZ(x), \quad (43)$$

where $c = a/b$; $Z(x) = exp(z(x)/b)$. Eq. (43) is solved in terms of standard Lambert W-function [29] as

$$Y = \frac{1}{c}W(cZ(x)), \quad (44)$$

which leads, in the expanded form, to

$$P_{H_2} = \frac{RT}{2\lambda}W\left(\frac{2\lambda P_{ref}}{RT}e^{-\frac{2z(x)}{RT}}\right). \quad (45)$$

Both Eqs. (40) and (45) are, in principle, discontinuous at the phase transition points x_α and x_β. From a physical point of view it is, however, obvious that the isotherms must be continuous. In order to obtain continuous dependencies in Eq. (45), the following restrictions are imposed to preserve the continuity of $P_{H_2}(x)$ at x_α and x_β

$$\lim_{x\uparrow x_\alpha} P_{H_2}(x) = \lim_{x\downarrow x_\alpha} P_{H_2}(x) \quad \text{and} \quad \lim_{x\uparrow x_\beta} P_{H_2}(x) = \lim_{x\downarrow x_\beta} P_{H_2}(x). \quad (46)$$

No volume expansion

Now the general state equation has been derived (Eq. (39)) it is interesting to theoretically investigate the impact of the materials volume expansion on the simulated isotherms. In this specific case, the volume expansion in both the solid solution and two-phase coexistence regions is considered negligible and all volume-related terms can therefore be neglected. Consequently, function λ defined by Eq. (40) is reduced to zero. The final state equation can then be significantly simplified to

$$\frac{1}{2}RT\ln\frac{P_{H_2}}{P_{ref}} = -\frac{9}{4}RT - T\left(s_H - \frac{1}{2}Rs_0\right) + F\begin{cases} \varepsilon_H + L, & x_\alpha \le x \le x_\beta \\ \varepsilon_H, & otherwise \end{cases}, \quad (47)$$

Substituting the expressions for s_H (Eq. (19)) and ε_H (Eq. (16)) into Eq. (47) an explicit expression is obtained for the partial hydrogen pressure as a function of the normalized hydrogen concentration in the hydride-forming material

$$P_{H_2} = P_{ref}\exp\left(-\frac{9}{2} + s_0\right) \times exp\begin{cases} \frac{2F}{RT}(E_\alpha + U_{\alpha\alpha}x) - 2\ln\left(\frac{1-x}{x}\right), & x < x_\alpha \\ \frac{2F}{RT}\frac{E_\beta x_\beta - E_\alpha x_\alpha - U_{\alpha\alpha}x_\alpha^2(N_\alpha/n_{max}) + U_{\beta\beta}x_\beta^2(N_\beta/n_{max})}{x_\beta - x_\alpha} + \frac{2F}{RT}\frac{U_{\alpha\beta}x_\alpha x_\beta(N_\alpha/n_{max} - N_\beta/n_{max})/2}{x_\beta - x_\alpha} + \frac{2FL}{RT} - 2\frac{S_\alpha^0 - S_\beta^0}{x_\beta - x_\alpha}, & x_\alpha \le x \le x_\beta \\ \frac{2F}{RT}(E_\beta + U_{\beta\beta}x) - 2\ln\left(\frac{1-x}{x}\right), & x > x_\beta \end{cases} \quad (48)$$

To preserve pressure continuity at the phase transition points in Eq. (48), Eq. (46) can be applied which, after simplification, gives the following continuity conditions

$$\begin{cases} L = \dfrac{D_{\alpha\beta} - D_\alpha - D_\beta + E_\alpha + E_\beta + U_{\alpha\alpha}\mathrm{x}_\alpha + U_{\beta\beta}\mathrm{x}_\beta}{2(\mathrm{x}_\beta - \mathrm{x}_\alpha)} - \dfrac{1}{(\mathrm{x}_\beta - \mathrm{x}_\alpha)^2}\left[E_\beta \mathrm{x}_\beta - E_\alpha \mathrm{x}_\alpha + \dfrac{U_{\beta\beta}\mathrm{x}_\beta^2 - U_{\alpha\alpha}\mathrm{x}_\alpha^2}{2}\right] \\ U_{\alpha\beta} = \dfrac{U_{\alpha\alpha}\mathrm{x}_\alpha^2 - U_{\beta\beta}\mathrm{x}_\beta^2}{\mathrm{x}_\alpha \mathrm{x}_\beta} - \dfrac{D_\alpha - D_\beta - E_\alpha + E_\beta - U_{\alpha\alpha}\mathrm{x}_\alpha + U_{\beta\beta}\mathrm{x}_\beta}{\mathrm{x}_\alpha \mathrm{x}_\beta}(\mathrm{x}_\beta - \mathrm{x}_\alpha) \end{cases}, \tag{49}$$

where $D_\alpha = \frac{RT}{F}\ln\left(\frac{1-\mathrm{x}_\alpha}{\mathrm{x}_\alpha}\right)$, $D_\beta = \frac{RT}{F}\ln\left(\frac{1-\mathrm{x}_\beta}{\mathrm{x}_\beta}\right)$, $D_{\alpha\beta} = \frac{RT}{F}(S_\alpha^0 - S_\beta^0)$.

Both the general state expression (Eq. (39)) and constant volume expression (Eq. (48)) offer the theoretical description of hydrogen absorption/desorption isotherms, allowing detailed parameter identification of complex hydrogen storage systems.

Volume expansion influence

The general expression for hydrogen absorption/desorption isotherms (Eq. (39)) also includes a volume expansion term, which is denoted as $P_{H_2}\lambda$, where λ is defined by Eq. (40). λ can be determined in three main crystallographic regions, which can be denoted as

$$\lambda(\mathrm{x}) = \begin{cases} \lambda_\alpha(\mathrm{x}), & \mathrm{x} \le \mathrm{x}_\alpha \\ \lambda_{\alpha\beta}(\mathrm{x}), & \mathrm{x}_\alpha \le \mathrm{x} \le \mathrm{x}_\beta \\ \lambda_\beta(\mathrm{x}), & \mathrm{x} \ge \mathrm{x}_\beta \end{cases}. \tag{50}$$

In the specific case that $\lambda_\alpha{=}\lambda_\beta{=}\lambda_{\alpha\beta}{=}0$ this corresponds to the constant volume situation considered before, which is covered by Eqs. (48) and (49). If λ deviates from zero, Eq. (39) still applies. However, the continuity conditions represented by Eq. (49) have to be replaced by the following expressions

$$\begin{cases} L(\lambda) = L + (\lambda_{\alpha\beta}(\mathrm{x}_\alpha) - \lambda_\alpha(\mathrm{x}_\alpha))P_\alpha + (\lambda_{\alpha\beta}(\mathrm{x}_\beta) - \lambda_\beta(\mathrm{x}_\beta))P_\beta \\ U_{\alpha\beta}(\lambda) = U_{\alpha\beta} + \dfrac{\mathrm{x}_\beta - \mathrm{x}_\alpha}{\mathrm{x}_\beta \mathrm{x}_\alpha}[(\lambda_{\alpha\beta}(\mathrm{x}_\alpha) - \lambda_\alpha(\mathrm{x}_\alpha))P_\alpha - (\lambda_{\alpha\beta}(\mathrm{x}_\beta) - \lambda_\beta(\mathrm{x}_\beta))P_\beta] \end{cases}, \tag{51}$$

where L and $U_{\alpha\beta}$ corresponds to the case that $\lambda{=}0$.

Van 't Hoff relationship

Considering the simplified case with no volume expansion, Eq. (47) can, for example, in the two-phase coexistence region be rearranged to

$$\frac{1}{2}\ln\frac{P_{H_2}}{P_{ref}} = \frac{F(\varepsilon_H + L) - \frac{9}{4}RT}{R}\frac{1}{T} - \frac{s_H - \frac{1}{2}Rs_0}{R}. \tag{52}$$

The reader will recognize in this expression the well-known Van 't Hoff relationship, which is generally represented by

$$\frac{1}{2}\ln\frac{P^\circ_{H_2}}{P_{ref}} = \frac{\Delta H^\circ}{R}\frac{1}{T} - \frac{\Delta S^\circ}{R}, \tag{53}$$

in which the molar enthalpy (ΔH^o) and entropy (ΔS^o) of the hydride (de-)formation reaction are considered to be temperature-independent [5,22]. The Van 't Hoff relation is generally determined in the middle of the two-phase coexistence region where $P^o_{H_2}$ holds. Considering the above mathematically derived expression (Eq. (52)), ΔH^o and ΔS^o can now be represented by

$$\Delta H = F(\varepsilon_H + L) - \frac{9}{4}RT, \tag{54}$$

and

$$\Delta S = s_H - \frac{1}{2}Rs_0. \tag{55}$$

In contrast to the classical Van 't Hoff equation (Eq. (53)), the molar enthalpy and entropy in the present derivation (Eq. (47)) are temperature-dependent and can be determined at any hydrogen concentration along the isotherms. Eq. (47) can therefore be considered as a generalization of the classical Van 't Hoff relationship, disclosing deeper insight into the microscopic properties of hydride-forming materials.

Heat capacity

Another important material characteristic is the heat capacity of hydride-forming materials (C_{MH}) which is generally expressed as the partial derivative of the internal energy of the solid with respect to temperature [25], according to

$$C_{MH} = \left(\frac{\partial U_{MH}}{\partial T}\right)_{V,P}, \tag{56}$$

where U_{MH} in the present terminology is the total internal energy of the solid, consisting of the energy of absorbed hydrogen (U_H in Eq. (13)) and energy of the host material (U_{Mi}, i=α,β in Eq. (22)), i.e. $U_{MH} = U_H + U_{M_\alpha} + U_{M_\beta}$. As a first approximation the partial derivative $\frac{\partial U_{MH}}{\partial T}$ can be represented as a finite difference between the internal energies at two different temperatures (T_1 and T_2). The heat capacity of Eq. (56) can then be rewritten as

$$C_{MH_{21}} = \frac{U_{MH_2} - U_{MH_1}}{T_2 - T_1}. \tag{57}$$

Results and discussion

Influence of volume expansion on the isotherms

Eq. (39) makes it possible to model the hydrogen equilibrium pressure as function of the amount of absorbed hydrogen, taking into account all processes, including the gas phase pressure and volumetric materials changes. Fig. 3 illustrates

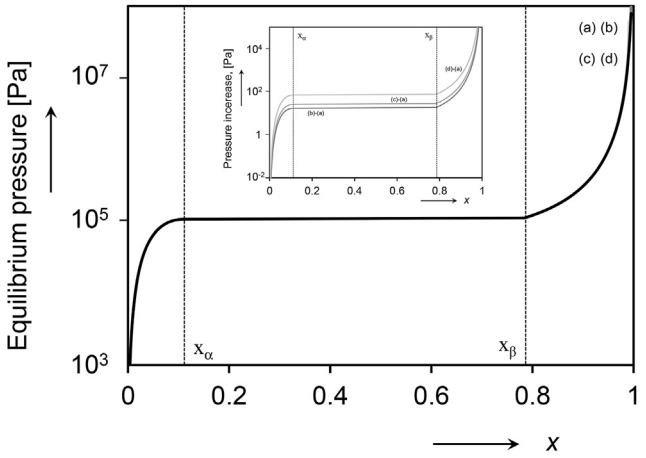

Fig. 3 – Pd-H isotherms simulated at 150 °C according to Eq. (39). Simulations without volume expansion (curve (a)) are compared with included volume expansions of 10% (curve (b)), 25% (curve (c)) and 100% (curve (d)). The insert shows pressure increase between curve (a) and curves (b), (c) and (d) accordingly. Corresponding curves are denoted as (b)–(a), (c)–(a) and (d)–(a).

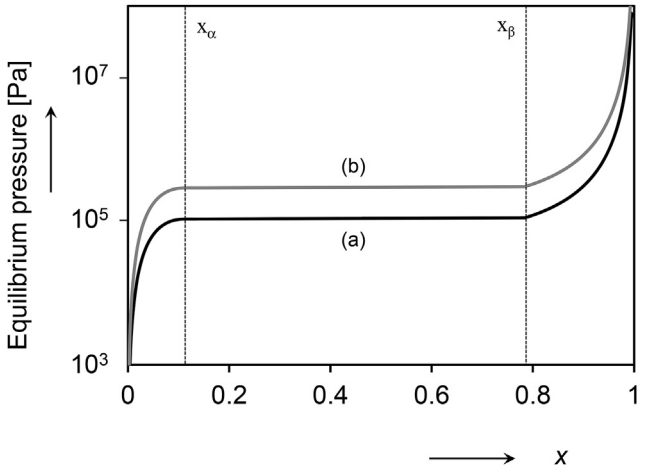

Fig. 4 – Pd-H isotherms simulated at 150 °C according to Eq. (39), considering (curve (a)) and not considering (curve (b)) a pressure contribution.

the influence of the volume expansion on the hydrogen absorption/desorption isotherms described by Eq. (39). The simulation results for Pd at 150 °C without volume expansion are shown in the black curve (a) using the analytical solution of Eqs. (48) and (49). The simulations including volume expansion are represented by the grey curves and are calculated from Eq. (39), using the W-Lambert function of Eq. (45). Curve (b) corresponds to the case of 10% volume expansion in the fully hydride PdH case, which visually coincides with curve (a). Assuming a volume expansion of 25%, similar to the fully hydride $LaNi_5H_6$ case (curve (c)) also hardly shows any deviation from curve (a). When a volume expansion of 100% is assumed, some small difference can be seen in the β solid solution region for pressures above 100 bar. The insert in Fig. 3 shows the pressure increase above curve (a) in more details. One can see that increase in the volume in general leads to increase in the pressure, and this pressure increase is proportional to the pressure as given by curve (a). This behavior is completely in line with the derivations of Appendix II, where it is shown that negative values of λ lead, *ceteris paribus*, to increasing pressure, see Eq. (A7).

It can therefore be concluded that for conventional hydride-forming materials at average temperatures and pressures the influence of the volume expansion on the isotherms is negligibly small. Only when the volume expansions becomes larger than 100% a small pressure increase is to be expected but for most hydride-forming materials these are unrealistic expansion values.

Influence of pressure on the isotherms

The pressure-related terms appear in the expression for the Gibbs free energy of Eq. (38). In the previously developed models the influence of the pressure on the isotherms has not been taken into account. The presence of the pressure-related terms in the final equations gives more physically realistic values for both the microscopic and macroscopic parameters. Fig. 4 shows, as an example, the simulated isotherm of Pd at 150 °C with (curve (a)) and without (curve (b)) considering the influence of the hydrogen pressure. Note that curve (a) in Fig. 4 is identical to curve (a) in Fig. 3. It can be concluded that the influence of the pressure is indeed quite significant and cannot be neglected in the mathematical description of isotherms.

Van 't Hoff relationship

Plotting the experimental values for $\frac{1}{2}\ln(P^0_{H_2}/P_{ref})$ as a function of the inverse temperature, the Van 't Hoff relationship for Pd is obtained as shown in Fig. 5a. From this linear dependence ΔH^0 and ΔS^0 can be calculated from the slope and intercept, respectively. The calculated experimental values for $\Delta H^0 = 42.40$ kJ mol^{-1} and $\Delta S^0 = 0.10$ kJ mol^{-1} K^{-1} are in close agreement with those reported before [30–32]. The molar enthalpy and entropy can also be calculated at the mid-plateau region for the simulated isotherms, using Eqs. (51) and (52). The average values obtained in the simulated temperature range are $\Delta H = 42.35$ kJ mol^{-1} and $\Delta S = 0.10$ kJ mol^{-1} K^{-1}, which are very close to the experimental values obtained from the classical Van 't Hoff expression Eq. (53).

Using the present model, the results for the Van 't Hoff equation can accurately be simulated at various hydrogen content. Fig. 5b illustrates the situation when these dependencies are plotted at the center of both the α (curve (b)) and β solid solution region (curve (c)), together with the mid-plateau region result (curve (a)). Obviously, curve (b) is below curve (a), as expected. Curve (c) is above curve (a), indeed indicating a steep increase of the partial hydrogen pressure in the solid solution region of the β-phase.

Isotherms

Desorption isotherms have been further simulated according to the above presented model without considering volume

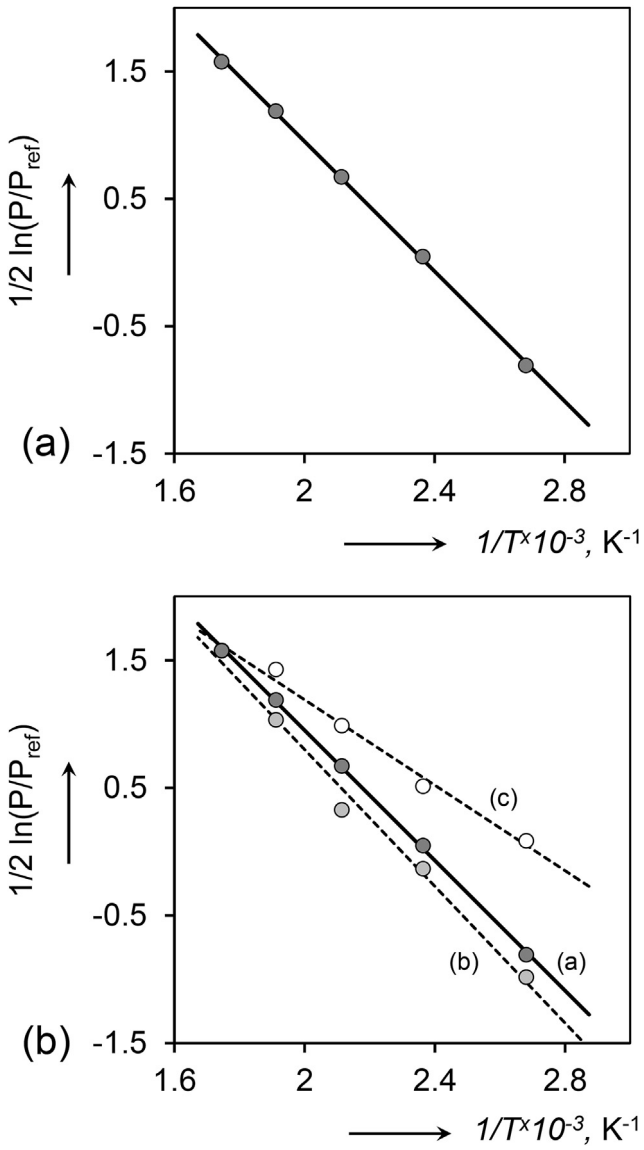

Fig. 5 – (a) The Van 't Hoff dependence for the experimentally determined Pd-H isotherms as a function of 1/T. (b) The calculated Van 't Hoff dependencies corresponding to the simulated mid-plateau region (curve (a)), at the center of the α-phase region (curve (b)) and at the center of the considered β-phase region (curve (c)).

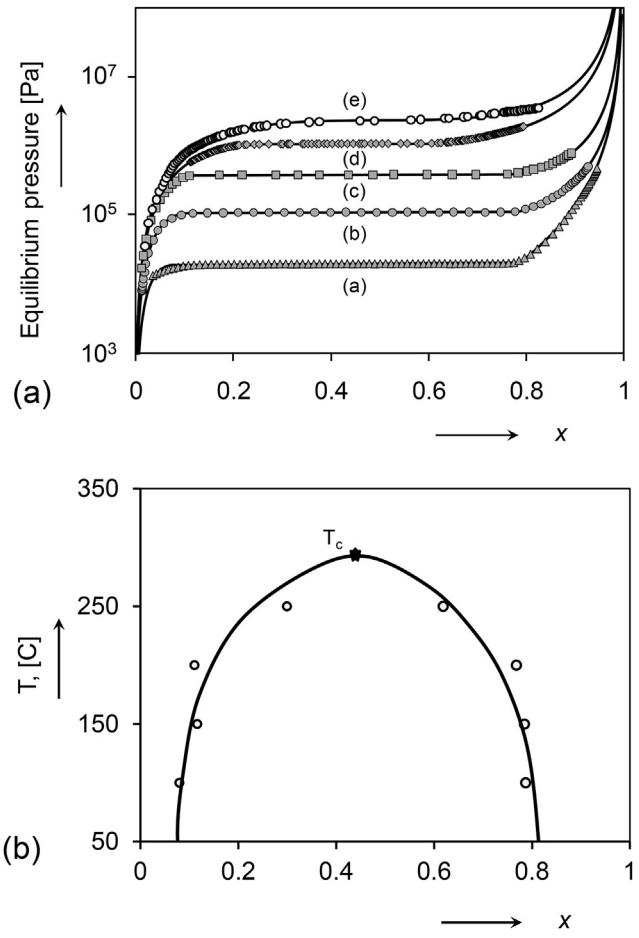

Fig. 6 – a. Simulation (lines) of experimentally measured Pd-H pressure-composition desorption isotherms (symbols) at various temperatures: 100 °C (a), 150 °C (b), 200 °C (c), 250 °C (d) and 300 °C (e). b. Temperature-composition phase diagram of Pd-H constructed based on the simulation results (a).

expansion as this influence appears to be rather limited. The simulation results will be compared with experimental results in this section. The experimental isotherms have been determined with conventional Sievert's type of equipment [33] on a variety of hydride-forming materials, *i.e.* at palladium powders in the temperature range of 100–300 °C, and at $LaNi_5$, $LaNi_{4.9}Al_{0.1}$, $LaNi_{4.7}Al_{0.3}$ and $La_{0.8}Ce_{0.2}Ni_5$ powders in the temperature range of 40–80 °C. All isotherms are normalized with respect to the absorbed hydrogen content (x).

Simulations of desorption isotherms of Pd-hydride at 100, 150, 200, 250 and 300 °C are shown in curves (a)-(e) of Fig. 6a, respectively. Excellent agreement between the experimental data (symbols) and simulations (lines) is found in all cases. These simulations are performed, using Eqs. (48) and (49) and assuming a constant sample volume during dehydrogenation, *i.e.* $\lambda = 0$. The isotherm simulated at 300 °C (curve (e)) is above the critical temperature (T_c) of Pd-hydride ($T_c = 293$ °C [30]) for which the two-phase coexistence region is absent. Obviously, the 300 °C isotherm has been simulated using the solid solution equations only, implying the first and third expression of Eq. (48). The model parameters have been determined by a non-linear least square method and the as-obtained values are listed in Table 1. The simulated phase diagram for the Pd-hydride system is shown in Fig. 6b. These results demonstrate that the miscibility gap is clearly influenced by the temperature. With increasing temperature the plateau pressures increase and the miscibility gap becomes narrower to finally disappear at T_c. Consequently, the Pd-hydride system only exhibits solid solution states at higher temperatures.

The chemical potentials of all species in the hydrogen storage system calculated by Eqs. (20), (24) and (29) for Pd at 150 °C are shown in Fig. 7a. The chemical potential of the hydrogen stored in the hydride-forming material is fully compensated by the chemical potential of hydrogen gas. The differential characteristics of Pd-H formation at 150 °C,

Table 1 – Parameters of the Pd-H hydrogen storage system. Optimized parameters are in bold.

N	Par	Dimension	100 °C	150 °C	200 °C	250 °C	300 °C
1	x_α	–	**0.079**	**0.116**	**0.110**	**0.299**	–
2	x_β	–	**0.787**	**0.784**	**0.768**	**0.618**	–
3	E^b_α	eV	**−0.041**	**−0.028**	**−0.017**	**−0.022**	**−0.021**
4	E^b_β	eV	**−0.206**	**−0.092**	**−0.043**	**−0.055**	–
5	$U^b_{\alpha\alpha}$	eV	**−0.448**	**−0.366**	**−0.306**	**−0.222**	**−0.196**
6	$U^b_{\beta\beta}$	eV	**0.014**	**−0.125**	**−0.184**	**−0.150**	–
7	$U^b_{\alpha\beta}$	eV	0.076	−0.904	−1.327	−0.419	–
8	$L\cdot10^2$	eV	7.364	2.134	0.306	1.193	–

enthalpy, entropy and Gibbs free energy (calculated from Eqs. (54) and (55)) are shown in Fig. 7b. The discontinuous behavior of the differential curves of the enthalpy and entropy are a clear indication of first-order phase-transitions [23,25]. However, these discontinuities at the phase transition points are of equal, but opposite magnitude, resulting in continuous Gibbs free energy curve and, consequently, isotherms. The singularities of the Gibbs free energy near $x = 0$ and $x = 1$ are caused by the entropy related terms $\ln\left(\frac{1-x}{x}\right)$ according to Eq. (19). The individual phase contributions to the entropy of formation are shown in Fig. 7c. As expected in solid solution regions, the total entropy (black curve) completely coincides with entropies of the corresponding phases. In two-phase coexistence region the total differential entropy is the summation of the partial increments of α- and β-phase.

Using the present model, the Gibbs free energies of the system components can be calculated in the integral form. The enthalpy, entropy and Gibbs free energy of the bulk of the hydride-forming material as a function of normalized hydrogen content for Pd at 150 °C are shown in Fig. 8. As expected, the contribution of the entropy to the Gibbs free energy is minor importance compared to that of the enthalpy (see Fig. 8a). Both contributions are continuous but not smooth and 'kinks' are clearly visible at the phase transition points, which corresponds to the discontinuities in the differential curves of Fig. 7b. For calculation of the above characteristics, the partial energies of host crystal lattice of the hydride-forming material in α- and β-phases (L_α and L_β, Eq. (23)) have been identified. It can simply be assumed that for the unhydrided host material the internal energy can be defined by the energy of α-phase unit cell, *i.e.* $U_M = L_\alpha$. The enthalpy of pure palladium can be found in literature (*e.g.* in Ref. [34]). Taking into account that for bulk material the internal energy is approximately equal to its enthalpy and using the value for $L = \frac{L_\beta - L_\alpha}{d}$ (see Table 1), L_α and L_β are determined to be 0.034 and 0.049 eV, respectively.

Heat capacity

The molar heat capacity for Pd at 150 °C simulated by Eq. (57) as a finite difference between 200 °C and 100 °C energy states is shown in Fig. 9. The heat capacity of pure palladium was assumed equal to that experimentally measured [34]. The difference in heat capacity between the non-hydrated and hydrated material is in a range reported in Ref. [35]. It is interesting also to observe the decline of the heat capacity at the end of the hydrating process.

Stoichiometric $LaNi_5$-based alloys

The desorption isotherms measured by the Sievert's type of equipment [33] for LaNi-based alloys at various temperatures have also been simulated in the present model. The comparison of the simulated and measured isotherms for $LaNi_5$ at 40, 60 and 80 °C are shown in Fig. 10. Excellent agreement between the simulation results (lines) and experimental data (symbols) is again found at all temperatures. The numerical values of model parameters for $LaNi_5$ were obtained by non-linear least squares method and are listed in Table 2. The Van 't Hoff lines for all measured hydride-forming materials considered in the present paper are shown in Fig. 11. The influence of the substitution metal on the isothermal properties of $LaNi_5$ can be clearly seen. Decreasing the Ni-content and increasing the Al-content results in a decrease of the plateau pressure, while adding Ce, replacing the La content in the AB_5-structure, results in an increase of the plateau pressure. The parameters based on the experimentally determined Van 't Hoff plot for $LaNi_5$ (Eq. (50)) are $\Delta H^0 = 31.22$ kJ mol^{-1}; $\Delta S^0 = 0.109$, kJ mol^{-1} K^{-1}. Parameter values obtained in the present simulations at the two-phase coexisting region are very close to those reported in literature [11,22,36].

Non-stoichiometric AB_x alloys

The performance of the proposed model is not restricted to materials with wide flat hydrogen absorption/desorption plateaus. Fig. 12 shows the isotherms for various non-stoichiometric $LaNi_{x-1}Cu$ alloys measured at 20 °C [13,14]. The copper content in these materials was fixed at $Cu_{1.0}$ but the overall non-stoichiometric AB_x composition was varied in the range of 5.0 and 6.0 by adjusting the Ni_{x-1} content. The experimental absorption and desorption isotherms are represented by the open and filled symbols, respectively. The lines represent the simulated isotherms, which in all cases are in good agreement with the experimental data. It is found that the isothermal pressures increase with increasing degree of non-stoichiometry. The stoichiometric $AB_{5.0}$ alloy (curves (d)) reveals wide and flat pressure plateaus. Simultaneously, the hysteresis between the absorption and desorption isotherms decrease to completely disappear for the $AB_{6.0}$ alloy (curves (d)), which is in line with the *in situ* XRD measurements for these alloys reported before [14]. Furthermore, the isotherms become much more sloping with increasing degree of non-stoichiometry. It can be concluded that the present model accurately describes a wide variety of alloys with various

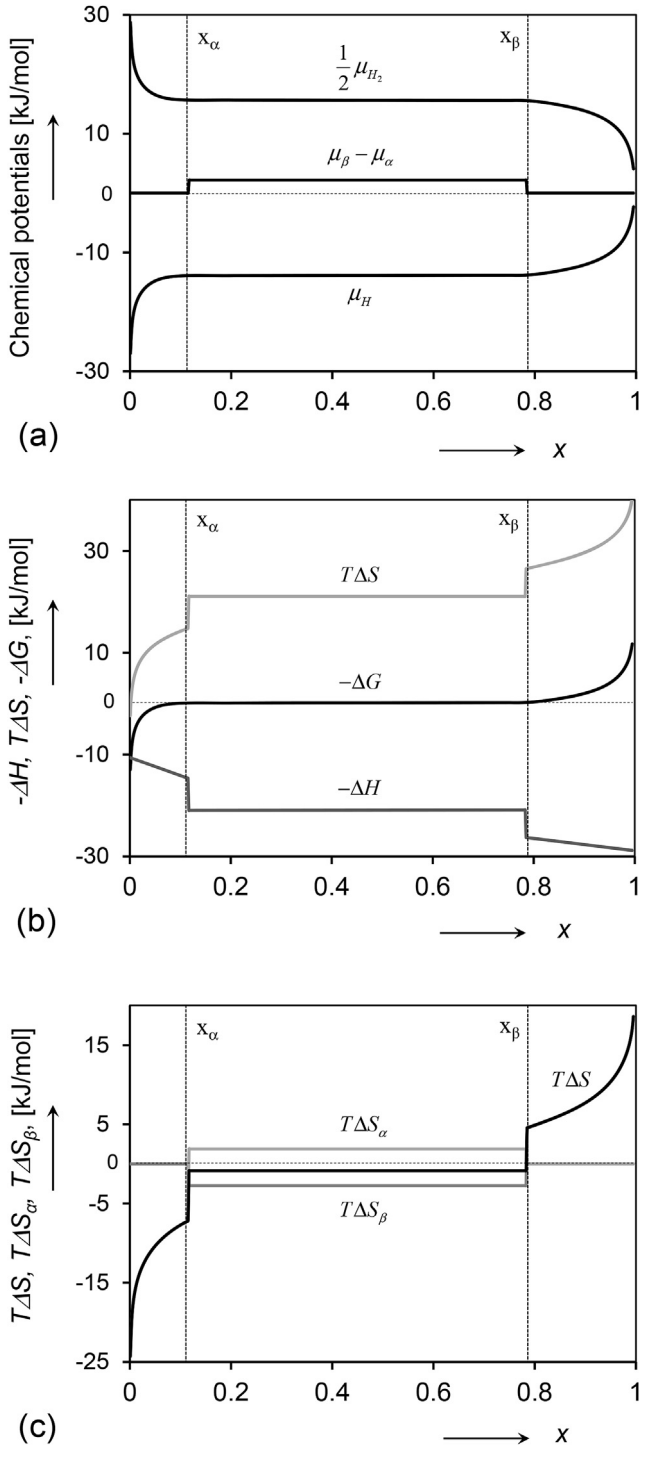

Fig. 7 – Simulation of Pd-H at 150 °C (a) various chemical potentials: hydrogen gas ($\frac{1}{2}\mu_{H_2}$), crystal lattice ($\mu_\beta - \mu_\alpha$) and absorbed hydrogen (μ_H); (b) differential molar characteristics of hydride formation: enthalpy ($-\Delta H$), entropy ($T\Delta S$) and Gibbs free energy ($-\Delta G$); (c) total molar entropy of hydride formation ($T\Delta S$) and its α- ($T\Delta S_\alpha$) and β- ($T\Delta S_\beta$) phase contributions.

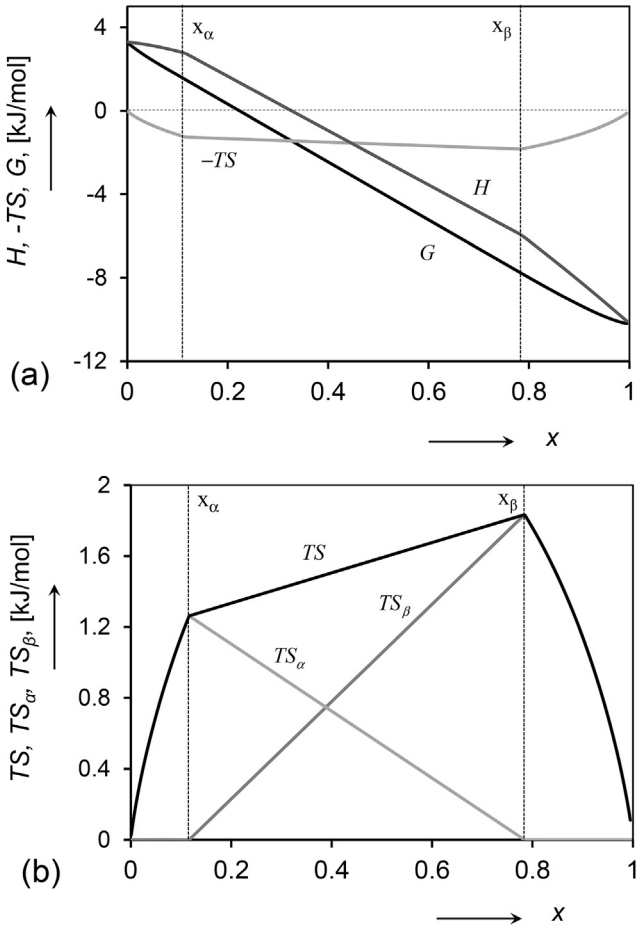

Fig. 8 – Simulation of Pd-H at 150 °C (a) integral molar characteristics of hydride formation: enthalpy (H), entropy ($-TS$) and Gibbs free energy (G); (b) total molar entropy of hydride formation (TS) and its α- (TS_α) and β- (TS_β) phase contributions.

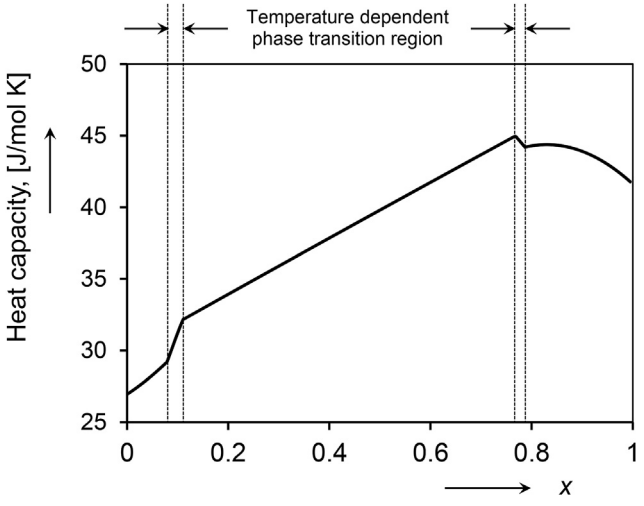

Fig. 9 – Simulated heat capacity of palladium at 150 °C as a function of hydrogen content.

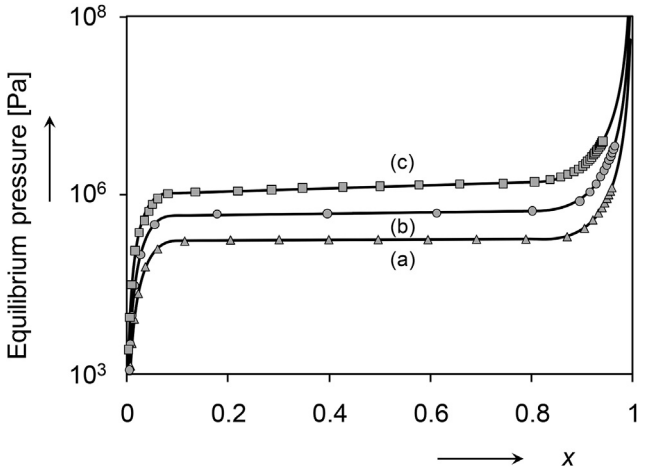

Fig. 10 – Simulation (lines) of experimentally measured $LaNi_5$-H pressure-composition isotherms (points) at various temperatures: 40 °C (a), 60 °C (b) and 80 °C (c).

Table 2 – Parameters of the $LaNi_5$ hydrogen storage system. Optimized parameters are in bold.

N	Par	Dimension	40 °C	60 °C	80 °C
1	x_α	–	**0.098**	**0.091**	**0.081**
2	x_β	–	**0.808**	**0.809**	**0.819**
3	E_α^b	eV	**−0.018**	**−0.008**	**0.004**
4	E_β^b	eV	**0.004**	**0.003**	**0.006**
5	$U_{\alpha\alpha}^b$	eV	**−0.304**	**−0.346**	**−0.405**
6	$U_{\beta\beta}^b$	eV	**−0.186**	**−0.183**	**−0.184**
7	$U_{\alpha\beta}^b$	eV	−1.580	−1.688	−1.944
8	$L\cdot10^2$	eV	−2.428	−1.966	−1.744

characteristics, including sloping plateaus and hysteresis effects. This makes the proposed model universal to describe hydrogen absorption and desorption processes of hydride-forming compounds.

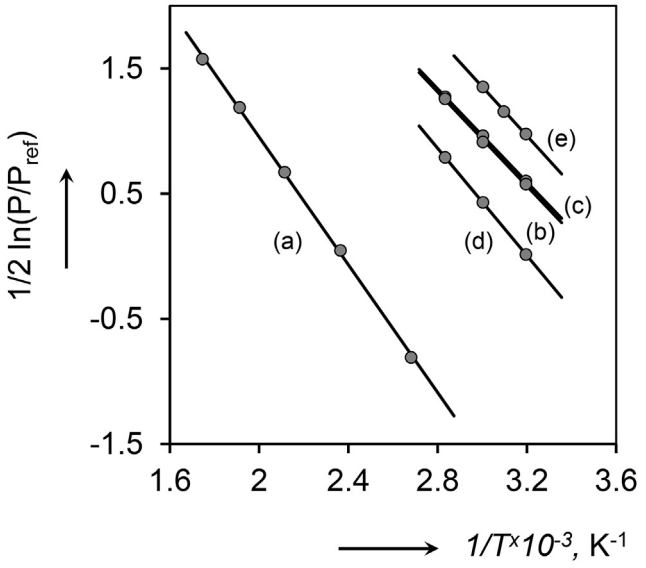

Fig. 11 – Van 't Hoff lines for Pd (a), $LaNi_5$ (b), $LaNi_{4.9}Al_{0.1}$ (c), $LaNi_{4.7}Al_{0.3}$ (d) and $La_{0.8}Ce_{0.2}Ni_5$ (e).

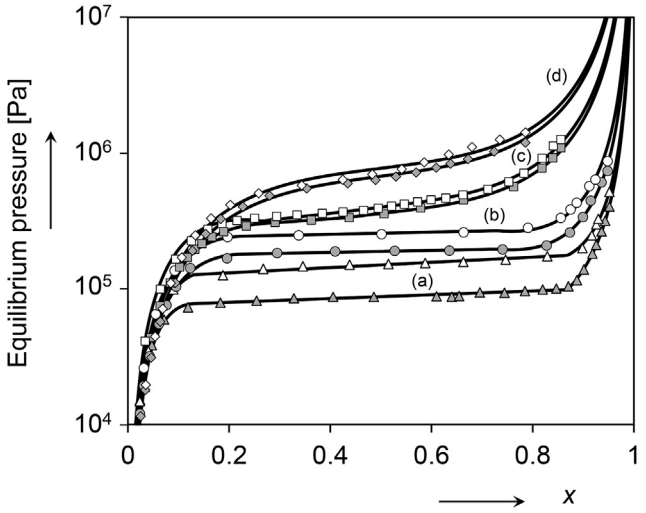

Fig. 12 – Pressure-composition isotherms for non-stoichiometric $LaNi_{x-1}Cu$ alloys at 20 °C. Symbols represent the experimental data and lines the simulations. Open and filled symbols refer to the absorption and desorption isotherms, respectively for $LaNi_{4.0}Cu$ (a), $LaNi_{4.2}Cu$ (b), $LaNi_{4.4}Cu$ (c) and $LaNi_{5.0}Cu$ (d).

Conclusions

A new mathematical model has been presented, describing the thermodynamics of hydrogen storage systems. The model is based on first principles of chemical and statistical thermodynamics and consists of a detailed description of all parts in the system, including the host metal, hydrogen absorbed in the various crystallographic phases of the host material, and hydrogen in the gas phase. Considering the energy, the Gibbs free energy and the chemical potential as a function of hydrogen content of each component in the system results in a general state equation, describing temperature-dependent isotherms. Conclusively, the equilibrium hydrogen pressure can be accurately simulated as a function of hydrogen content in the bulk of hydride-forming materials, taking into account the gas pressure and the volume expansion of the host material.

The simulation results of desorption isotherms at various temperatures have been compared with the experimental results obtained for Pd, $LaNi_5$, $LaNi_{4.9}Al_{0.1}$, $LaNi_{4.7}Al_{0.3}$ and $La_{0.8}Ce_{0.2}Ni_5$. The simulation results were found to be in good agreement with the experimental results. The model was able to calculate values of enthalpy (ΔH) and entropy (ΔS) of hydride-formation as a function of hydrogen content and the results were found to be in good agreement with the classical experimental Van 't Hoff dependence. Using the model parameters at various temperatures, the heat capacity of the hydride-forming materials has been simulated of hydrogen content. The theoretically predicted heat capacity of Pd was also found to be in good agreement with experimental results reported in literature. In addition it has been shown that sloping plateaus and hysteresis between the absorption and desorption isotherms also can be accurately modeled.

Acknowledgments

The second and the last authors were supported by ENIAC/ECSEL projects BATTMAN and 3Ccar.

Appendix I

Derivation of the chemical potential of hydrogen in the gas phase

For the reversible change of state of gases the first thermodynamic law holds [25]:

$$dU = TdS - pdV, \tag{A1}$$

where U is the internal energy of the gas atoms/molecules, T is the temperature, S entropy p pressure and V is volume. The state equations for the diatomic hydrogen gas can be represented by Refs. [6,24,28].

$$U = \frac{5}{2}NkT,\ pV = NkT, \tag{A2}$$

where k is Bolzmann constant; N is the number of gas atoms.

Taking into account the general gas law [23,25], substituting Eq. (A2) into Eq. (A1) and integrate it from the reference state (T_0, P_0), the following expression is obtained

$$S(N,T,p) = Nk\left[s_0 + \ln\left\{\left(\frac{T}{T_0}\right)^{7/2}\left(\frac{p_0}{p}\right)\right\}\right], \tag{A3}$$

where $s_0 = \frac{S_0(T_0,V_0)}{Nk}$ and $S_0(T_0,V_0)$ is the reference entropy of hydrogen. Furthermore, it is known that [28].

$$\left.\frac{\partial S}{\partial N}\right|_{U,V} = -\frac{\mu}{T}, \tag{A4}$$

where μ is chemical potential of gas.

Applying the following notations [6,7]: $\mu = \mu_{H_2}$, $p = P_{H_2}^{eq}$ and $p_0 = P_{ref}$, introducing $R = kN_a = k\frac{F}{e}$, and differentiating Eq. (A3) for isothermal conditions according to Eq. (A4) taking into account Eq. (A2) one can obtain equation of the chemical potential of diatomic hydrogen gas

$$\mu_{H_2} = RT\left(\frac{7}{2} - s_0\right) + RT\ln\frac{P_{H_2}^{eq}}{P_{ref}}. \tag{A5}$$

Appendix II

Sensitivity of equilibrium hydrogen pressure on λ

It will be shown in this Appendix that there is a theoretical reason that a decrease in λ results in higher equilibrium pressures. Consider function

$$f(P_{H_2},\lambda) = -\frac{RT}{2} - \frac{1}{2}\left(RT\left(\frac{7}{2} - s_0\right) + RT\ln\frac{P_{H_2}}{P_{ref}}\right) + F\varepsilon_H - Ts_H - P_{H_2}\lambda + \begin{cases} FL, & x_\alpha \le x \le x_\beta \\ 0, & otherwise \end{cases}.$$

According to Eq. (39), $f(P_{H_2},\lambda) = 0$ for all (small) deviations of λ and P_{H_2} from certain given (initial) value for λ and P_{H_2}. Consequently,

$$df(P_{H_2},\lambda) = \frac{\partial f}{\partial P_{H_2}}dP_{H_2} + \frac{\partial f}{\partial \lambda}d\lambda = -\frac{RT}{2}\frac{dP_{H_2}}{P_{H_2}} - P_{H_2}d\lambda - \lambda dP_{H_2} = 0, \tag{A6}$$

and therefore

$$\frac{dP_{H_2}}{d\lambda} = -\frac{P_{H_2}}{\frac{RT}{2P_{H_2}} + \lambda}. \tag{A7}$$

Consider the constant volume case when $\lambda = 0$, then Eq. (A7) results in $\frac{dP_{H_2}}{d\lambda} = -\frac{2(P_{H_2})^2}{RT} < 0$. Therefore, small but negative values for λ will always result in higher equilibrium hydrogen pressure, which is in agreement with the results shown in Fig. 3.

REFERENCES

[1] Fukai Y. The metal-hydrogen system. Berlin: Springer-Verlag; 1993.
[2] Notten PHL, Latroche M. Nickel-metalhydride batteries: a successful application of hydrogen storage materials. In: Garche J, editor. Encyclopedia of electrochemical power sources. Amsterdam: Elsevier; 2009. p. 502–21.
[3] Flanagan TB. Thermodynamics of metal-gas reactions. In: Grandjean F, Long GJ, Buschow KHJ, editors. Interstitial intermetallic alloys. Dordrecht: Kluwer Acad. Publish; 1995. p. 43–76. Chap. 4.
[4] Notten PHL. Rechargeable nickel-metalhydride batteries: a successful new concept. In: Grandjean F, Long GJ, Buschow KHJ, editors. Interstitial intermetallic alloys. Dordrecht: Kluwer Acad. Publish; 1995. p. 151–96. Chap. 7.
[5] Schlapbach L, Zuttel A. Hydrogen-storage materials for mobile applications. Nature 2002;414:353–8.
[6] Ledovskikh A, Danilov D, Notten PHL. Modeling of hydrogen storage in hydride-forming materials: equilibrium gas-phase kinetics. Phys Rev B 2007;76. 064106(1-16).
[7] Ledovskikh A, Danilov D, Rey WJJ, Notten PHL. Modeling of hydrogen storage in hydride-forming materials: statistical thermodynamics. Phys Rev B 2006;73. 014106(1-12).
[8] Griessen R, Riesterer T. Heat formation models. In: Schlapbach L, editor. Topics in applied physics. Berlin: Springer-Verlag; 1988. p. 219–84.
[9] Frieske H, Wicke E. Magnetic susceptibility and equilibrium diagram of PdH_n. Ber. Bunsenges. Phys Chem 1973;77:48–52.
[10] Flanagan TB, Oates WA. Hydrogen in intermetallic compounds I. In: Schlapbach L, editor. Topics in applied physics. Berlin: Springer-Verlag; 1988. p. 49–85.
[11] Luo S, Flanagan TB, Notten PHL. Thermodynamic properties of non-stoichiometric $LaNi_{x-1}Cu$-H systems. J Alloys Compd 1996;239:214–25.
[12] Notten PHL, Daams JLC, De Veirman AEM, Staals AA. *In situ* X-ray diffraction: a useful tool to investigate hydride formation reactions. J Alloys Compd 1994;209:85–91.
[13] Notten PHL, Einerhand REF, Daams JLC. On the nature of the electrochemical cycling stability of non-stoichiometric $LaNi_5$-based hydride-forming compounds Part I. crystallography and electrochemistry. J Alloys Compd 1994;210:221–32.
[14] Notten PHL, Einerhand REF, Daams JLC. On the nature of the electrochemical cycling stability of non-stoichiometric

$LaNi_5$-based hydride-forming compounds Part II. *In situ* x-ray diffractometry. J Alloys Compd 1994;210:233–41.
[15] Vermeulen P, Ledovskikh A, Danilov D, Notten PHL. Thermodynamics and kinetics of the thin film magnesium-hydrogen system. Acta Mater 2009;57:4967–73.
[16] Lacher JR. The statistics of the hydrogen-palladium system. Proc Cambr Phil Soc 1937;33:518–23.
[17] Evans MJB, Everett DH. Thermodynamics of the solution of hydrogen and deuterium in palladium. J Less-Common Met 1976;49:123–45.
[18] Lototsky MV, Yartys VA, Marinin VS, Lototsky NM. Modelling of phase equilibria in metal–hydrogen systems. J Alloys Compd 2003;356–357:27–31.
[19] McKinnon WR, Haering RR. Physical mechanisms of intercalation. In: White RE, Bockris JM, Conway BE, editors. Modern aspects of electrochemistry, vol. 15. New York: Springer-Verlag; 1983. p. 235–304. Chap. 4.
[20] Naito S, Yamamoto M, Doi M, Kimura M. Sloping plateaux in the pressure–composition isotherms of the titanium–hydrogen and $Ti_{94}Al_6$–hydrogen systems. J Chem Soc, Far Trans 1995;91:4143–7.
[21] Kalisvaart P, Vermeulen P, Ledovskikh A, Danilov D, Notten PHL. The electrochemistry and modelling of hydrogen storage materials. J Alloys Compd 2007;446–447:648–54.
[22] Sandrock G. A panoramic overview of hydrogen storage alloys from a gas reaction point of view. J Alloys Compd 1999;293–295:877–88.
[23] Atkins P, De Paula J. Atkins' physical chemistry. 9th ed. New York: Oxford University Press; 2006.
[24] Kubo R. Thermodynamics: an advanced course with problems and solutions. Amsterdam: Elsevier; 1968.
[25] Castellan GW. Physical chemistry. Reading, MA: Addison-Wesley; 1983.
[26] Alberty RA. Use of legendre transforms in chemical thermodynamics (IUPAC technical Report). Pure Appl Chem 2001;73:1349–80.
[27] Hill TL. An introduction to statistical thermodynamics. Reading, MA: Addison-Wesley; 1960.
[28] Greiner W, Neise L, Stocker H. Thermodynamics and statistical mechanics. New York: Springer-Verlag; 1995.
[29] Corless RM, Gonnet GH, Hare DE, Jeffrey DJ, Knuth DE. On the Lambert W function. Adv Comput Maths 1996;5:329–59.
[30] Manchester FD, San-Martin A, Pitre JM. The H-Pd (hydrogen-palladium) system. J Phase Equilibria 1994;15:62–83.
[31] Flanagan TB, Luo W, Clewley JD. Calorimetric enthalpies of absorption and desorption of protium and deuterium by palladium. J Less-Comm Met 1991;172–174:42–55.
[32] Burch R. The adsorption and absorption of hydrogen by metals. In: Roberts MW, Thomas JM, editors. Chemical physics of solids and their surfaces, vol. 9. London: Royal Soc. Chem; 1979. p. 1–17.
[33] PCT-Pro-2000. Installation and operations manual. Newark: Hy-Energy LLC; 2007.
[34] Cordfunke EHP, Konnings RJM. The high temperature thermophysical properties of ruthenium and palladium. Thermochim Acta 1989;139:99–106.
[35] Gamberale L, Garbelli D, Piana G. Measurement of heat capacity of PdH_x. In: Li XZ, editor. Proceedings of the 9th international conference on cold fusion; 2002. p. 105–8. Beijing: China.
[36] Ohlendorf D, Flotow HE. Heat capacities and thermodynamic functions of $LaNi_5$, $LaNi_5H_{0.36}$ and $LaNi_5H_{6.39}$ from 5 to 300 K. J Less-Comm Met 1980;73:25–32.